Turkish Journal of Electrical Engineering & Computer Sciences

http://journals.tubitak.gov.tr/elektrik/

Research Article

Turk J Elec Eng & Comp Sci
(2018) 26: 1860 – 1870
© TÜBİTAK
doi:10.3906/elk-1711-407

SAR image denoising based on patch ordering in nonsubsample shearlet domain

Shuaiqi LIU[1,2,3,*], **Qi HU**[1,2,3], **Pengfei LI**[1,2,3], **Jie ZHAO**[1,2,3], **Zhihui ZHU**[4]
[1]College of Electronic and Information Engineering, Hebei University, Baoding, P.R. China
[2]Machine Vision Engineering Research Center of Hebei Province, Baoding, P.R. China
[3]Key Laboratory of Digital Medical Engineering of Hebei Province, Baoding, P.R. China
[4]Department of Electrical Engineering and Computer Science, Colorado School of Mines, Golden, CO, USA

Received: 29.11.2017 • **Accepted/Published Online:** 11.04.2018 • **Final Version:** 27.07.2018

Abstract: Synthetic aperture radar (SAR) has been extensively adopted in a variety of fields, e.g., agriculture and marine fields. In this regard, the improvement of SAR image quality has aroused a wide concern worldwide. In recent years, image processing based on local patches has been very popular and proven feasible. In this paper, a novel SAR image denoising algorithm is proposed in the NSST domain on the basis of patch ordering. First, the shearlet transform is applied to logarithmic transformation of the noisy SAR image. Second, the coefficients of the shearlet are denoised respectively by combining patch ordering and 1D filtering. Finally, the denoised SAR image can be obtained by exponential transformation after applying the inverse shearlet to denoised coefficients. The experimental results show that the proposed method not only effectively suppresses the speckle noise and improves the PSNR and ENL of denoising the SAR images but also obviously improves the visual effects of the SAR images, especially in maintaining the image edge and texture information.

Key words: Synthetic aperture radar image denoising, nonsubsampled shearlet transform, patch ordering

1. Introduction

As a coherent imaging system, synthetic aperture radar (SAR) can produce high-resolution microwave-based remote sensing images in any weather and at any time of day. In contrast to visible light, it will not be obstructed by harsh conditions, inclusive of season, weather, and lighting. Additionally, the SAR image takes on numerous advantages, e.g., multiband, multipolarization, variable side view, and strong penetrability. Accordingly, SAR images have been extensively recognized by many countries worldwide and have been adopted in a wide range of fields, including home and military applications. However, by virtue of the coherent imaging mechanism, the homogeneous regions within the image taking on identical back scattering coefficients would present homogeneous granular noise (which is called coherent noise). Accordingly, the subsequent processing of SAR images is seriously affected [1–3]. In this regard, SAR image denoising primarily aims to suppress or eliminate the coherent noise. Two methods are mostly adopted to denoise SAR image: spatial filtering algorithms and transform domain filtering algorithms.

The spatial filtering denoising methods include the Lee filter [3], Frost filter [4], nonlocal means denoising [5], and so on. Transform domain filtering algorithms refer to the denoising algorithms based on wavelet transform and multiscale geometric transform, such as Bayesian denoising in the wavelet domain [6], SAR

*Correspondence: shdkj-1918@163.com

image denoising in the contourlet domain [7], and SAR image denoising in the shearlet domain [8]. Given that spatial filtering denoising algorithms may make the SAR image dark easily, the denoising algorithms based on the transform domain are the mainstream denoising algorithms. As wavelet transform takes on preferable time-frequency characteristics, it is being employed more broadly to denoise SAR images. However, the wavelet transform cannot represent the image optimally, which affects the denoising effect. To better present two-dimensional images with line or surface singularity and overcome the nonsparsity and the lack of direction selectivity in high-dimensional coefficients caused by using wavelets, many multiscale geometry transforms have been proposed, such as contourlet, curvelet, shearlet, etc. Among them, the shearlet is a new transform with the advantages of contourlet and curvelet, which is constructed by a synthetic inflated affine system and overcomes the shortcomings of contourlet and curvelet transforms [9–11]. This transform is not only theoretically consistent with multiresolution analysis but also represents an image sparsely to produce optimal approximation. It has flexible direction selectivity and can be implemented easily. Thus, the shearlet transform has been applied to many fields since it was first proposed. In this paper, the nonsubsampled shearlet transform (NSST) in [10] is adopted to reduce speckle in SAR images.

Image processing with local patches has been frequently adopted and proven highly efficient in recent years. The crux of the algorithms based on patches is the same: first and foremost, all possible overlapping patches are to be extracted by dividing the given image, and these patches are comparatively small compared with the original image size (a typical patch size would be 8×8 pixels); secondly, the image can be processed by operating these patches by adopting their relationships; and finally, the manipulated patches (or sometimes only their center pixels) are put back to origin positions to form the final resulting image.

In summary, the most important point of image processing algorithms based on patches is to factor in how patches are related to each other and to process an image whereby such a relationship exists. For example, NL-means does weighted averaging denoising of pixels by using surrounding patches that have nonlocal similarity [11]; in others, the patches can be clustered into disjoint subsets and each subset is processed differently [12–14]. Image processing algorithms based on sparse representation and low rank matrices [15–17] are a class of algorithms based on patches. As indicated by many foregoing algorithms, this work seeks to find similar patches extracted elsewhere in the image to match the patch taken from the image. In this regard, each image patch can take on a highly structured geometric form in its embedded space. Through reckoning with the nonlocal patch set, the final reestablished image is attained whereby position restoration occurs. This type of algorithm in patch matching and processing is very time-consuming, though these algorithms have a good effect on the processed image. Patch sets are treated by most of the algorithms as being random and independent. Apparently, this does not represent the actual situation. Ram et al. in [18] thus established a wavelet frame based on patch ordering. The image patches in the transform domain are ordered abiding by certain rules, and simple one-dimensional (1D) filtering can then be adopted to filter the relevant patch sets, which not only simplifies the computation substantially but also processes the image better.

Accordingly inspired, we propose a novel SAR image denoising algorithm based on the NSST with patch ordering. This algorithm operates the patch ordering to the NSST decomposition coefficient, and the optimal filtering coefficients associated with image patches can be attained by using the least square method. Accordingly, a better denoised effect can be attained. As indicated in the experimental results, the proposed algorithm outperforms other traditional denoising algorithms.

The paper is organized as follows: in Section 2, we give the mathematical theory of shearlets and the construction method of the NSST. In Section 3, we introduce the SAR image denoising algorithm based on

patch ordering in the NSST domain. In Section 4, we present the experimental results, which demonstrate the advantages of the proposed algorithm. We give some conclusions in Section 5.

2. Nonsubsample shearlet transform

The synthetic wavelet is the theoretical basis of shearlet transform. When dimension $n = 2$, shearlet functions can be generated by affine transform as follows:

$$\Psi_{AB}(\psi) = \left\{ \psi_{j,l,k}(x) = |\det A|^{j/2} \psi\left(B^l A^j x - k\right) : j, l \in Z, k \in Z^2 \right\}, \tag{1}$$

where $\psi \in L^2\left(R^2\right)$, A and B are 2×2 invertible matrices, and $|\det B| = 1$.

If $\Psi_{AB}(\psi)$ constitutes a Parseval frame for any $f \in R^2$, the element of $\Psi_{AB}(\psi)$ is called a synthetic wavelet. This work asserts that A^j is a telescopic transform matrix and B^j is a geometric transform matrix of the preservative region. $A = A_0 = \begin{bmatrix} 4 & 0 \\ 0 & 2 \end{bmatrix}$ is an anisotropic expansion matrix, and $B = B_0 = \begin{bmatrix} 1 & 1 \\ 0 & 1 \end{bmatrix}$ is a shear matrix.

If $f \in L^2\left(R^2\right)$, the continuous shearlet transform can be defined as follows:

$$SH_\psi = \left\langle f, \psi_{j,l,k}^{(d)} \right\rangle, \tag{2}$$

where $j \geq 0$, $l = -2^j \sim 2^j - 1$, $k \in Z^2$, and $d = 0, 1$.

NSST [10] refers to an extension of the shearlet transform, compensating for its defective translational robustness and marginal pseudo-Gibbs distortion. It is realized by multiscale transform and multidirection transform. In the first part, the image is decomposed by a nonsubsampled pyramid (NSP). Through the k-layer decomposition, the NSP is able to generate $k + 1$ subimages of the same size as the original image, including k high-frequency images and a low-frequency image. In the second part, the shear filter is applied to achieve multidirection transformation. The standard shear filter is effectuated in a pseudopolarized grid by translating the window function, whereas the NSST maps the filter to a Cartesian coordinate system. This approach avoids the downsampling operation and thus satisfies the translation invariance. Through applying the NSST to denoise the image, not only can noise be evidently reduced, but also more information of the source image can be retained.

3. SAR image denoising based on patch ordering in the NSST domain

3.1. The basic scheme

In [19], to utilize the global sparsity of an image more effectively and efficiently, the authors proposed patch ordering in light of redundant tree-based wavelet transform, and its application better solves the inverse problem existing in the image. Inspired by this, a new NSST decomposition scheme is established by adopting the patch ordering, as shown in Figure 1.

a^ℓ and d^ℓ in Figure 1 denote the low-frequency and high-frequency subband coefficients in ℓ-th scale range. P^ℓ denotes the ordering operator. $d^{\ell,p}$ denotes the high-frequency coefficient after ordering. The operator P^ℓ in the proposed NSST decomposition scheme is different from the common NSST. Each operator P^ℓ generates a permutation $d^{\ell,p}$ of input vector d^ℓ. The operator P^ℓ can be interpreted as giving a linear

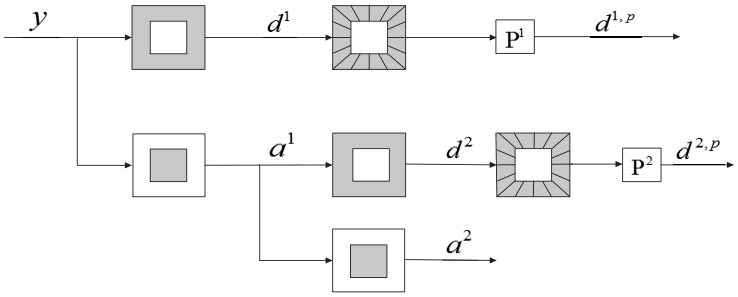

Figure 1. NSST decomposition scheme based on patch ordering.

single operator of the vector. It is adopted to smooth the coefficients of the different levels of the decomposition scheme. Thus, the new shearlet transform can represent an image globally and sparsely. Next, the solution of these operators from the image patches should be explored.

Similarly, the reconstruct scheme of the NSST can be established. The reordering operator $\tilde{\mathrm{P}}^{\ell}$ is adopted to reorder the coefficients. It reorders a vector and cancels the established order of P^{ℓ} and $\tilde{\mathrm{P}}^{\ell} = \left(\mathrm{P}^{\ell}\right)^{-1} = \left(\mathrm{P}^{\ell}\right)^{T}$. On that basis, the image is reestablished.

3.2. Building the permutation matrix

P

Let Y be an image of size $N_1 \times N_2$ where $N_1 N_2 = N$, and let Z be a noisy image. Let z and y denote the column stacked representations of Z and Y, respectively. Accordingly, the noisy image model is assumed to comply with:

$$z = y + v, \tag{3}$$

where v represents an additive white Gaussian noise, taking on zero mean and variance σ^2.

y_i and z_i are regulated to indicate the ith samples in vectors y and z, respectively. x_i is arranged to indicate the column stacking of the $\sqrt{n} \times \sqrt{n}$ patches around z_i in Z. Continuing the assumption in [19], the distance between patches x_i and x_j and the distance between the patches with center pixels i and j shall be proportional. To make the NSST represent the image globally and sparsely, it is necessary to sort patches x_i. The reordered patches make a smooth path, and the ordering signals y^p should be correspondingly smooth. The smoothness of the ordering signal y^p can be acquired by the following total variation:

$$\|y^p\|_{TV} = \sum_{j=2}^{N} |y^p(j) - y^p(j-1)|. \tag{4}$$

$\left\{x_j^p\right\}_{j=1}^{N}$ is regulated to denote the points after ordering $\{x_i\}_{i=1}^{N}$. It is explicit that the smoothness of the signal can be measured by the sum of path ω of points x_j^p and its neighboring points, which is established as:

$$X_{TV}^p = \sum_{j=2}^{N} \omega\left(x_j^p, x_{j-1}^p\right). \tag{5}$$

Minimizing X_{TV}^p, the ordering operators satisfying the requirements can be attained. This problem can be attributed to the shortest path problem whereby we should find a set of points x_i and only visit once for each

point. Thus, it is virtually a traveling salesman problem. In this paper, we use the algorithm in [19] to solve this problem. First, a square neighborhood encompassing each patch shall be sought. The size of the neighborhood is $B \times B$ patches. When all the patches in this neighborhood are visited, the patches that have not been visited for the entire image shall be overall operated to acquire the nearest neighborhood. This evidently simplifies the overall computation. For a detailed algorithm, please refer to [19]. It is clear that the operator P can be attained from the order of visiting.

3.3. 1D filtering

After obtaining the ordering operator, the NSST coefficient can be ordered to make the NSST coefficient present the image globally and optimally. Then the image can be better denoised by simple 1D filtering. Assume that the noise model is presented as in Eq. (3); in the meantime, y_i and z_i are arranged to denote the ith samples in vectors y and z, respectively. x_i indicates the column stacked of the $\sqrt{n} \times \sqrt{n}$ patches around z_i in Z. The flat region, edge, and texture of the image are sorted and filtered differently. First, the patches are split into two sets based on the standard deviation of the image: S_s, which involves the sets of smooth patches, and S_e, which comprises the sets of patches with edges or texture. Second, we apply the minimization in Eq. (5) to sets S_s and S_e to obtain two different ordering matrices, P_s and P_e. Finally, we can obtain $z^p_{j,s}$ and $z^p_{j,e}$ by sorting $z_{j,s}$ in subset S_s and $z_{j,e}$ in subset S_e based on P_s and P_e, respectively. That is:

$$\begin{bmatrix} z^p_{j,s} \\ z^p_{j,e} \end{bmatrix} = \begin{bmatrix} P_s\{z_{j,s}\} \\ P_e\{z_{j,e}\} \end{bmatrix} = \begin{bmatrix} \mathrm{P}_s \\ \mathrm{P}_e \end{bmatrix} z_j = \mathrm{P} z_j = z^p_j, \tag{6}$$

where the matrix $\mathrm{P} = \begin{bmatrix} \mathrm{P}_s \\ \mathrm{P}_e \end{bmatrix}$.

Obviously, the image can be denoised just by filtering $z^p_{j,s}$ and $z^p_{j,e}$. h_s and h_e are arranged to denote the filtering coefficients that are applied to $z^p_{j,s}$ and $z^p_{j,e}$. Then the denoising signal $\hat{y}_j$ can be attained as follows:

$$\hat{y}_j = \mathrm{P}^{-1} \begin{bmatrix} z^p_{j,s} h_s \\ z^p_{j,e} h_e \end{bmatrix} = \mathrm{P}^{-1} \begin{bmatrix} z^p_{j,s} & 0 \\ 0 & z^p_{j,e} \end{bmatrix} \begin{bmatrix} h_s \\ h_e \end{bmatrix} = \mathrm{P}^{-1} z^p_j h_j = Q_j h_j, \tag{7}$$

where $z^p_j = \begin{bmatrix} z^p_{j,s} & 0 \\ 0 & z^p_{j,e} \end{bmatrix}, h_j = \begin{bmatrix} h_s \\ h_e \end{bmatrix}, Q_j = \mathrm{P}^{-1} z^p_j$.

Then the filter coefficients $\hat{h}_j$ can be solved by the following equation:

$$\hat{h}_j = \arg\min_{h_j} \sum_{j=1}^{L} \|y_j - Q_j h_j\|^2 = \left[\sum_{j=1}^{L} (Q_j)^T Q_j \right]^{-1} \sum_{j=1}^{L} (Q_j)^T y_j, \tag{8}$$

where L denotes the number of image patches and y_j denotes a training set. The least squares method is adopted in this paper to solve Eq. (8) to obtain filter coefficients $\hat{h}_j$. Then, by Eq. (7), we can obtain the following:

$$\hat{y}_j = Q_j \hat{h}_j. \tag{9}$$

Similar to [19], the algorithm can be solved iteratively to optimize the experimental results.

3.4. SAR image denoising in the NSST domain

The proposed patch ordering-based denoising algorithm in the NSST domain can be extended to SAR image processing. In SAR imaging, each resolution unit on the ground can count as numerous scattering points with different distances to the radar receiver. The phase and amplitude of the echoes emitted by each scattering center are independent; thus, the amplitude and phase of the overall echo signal are also randomly given. The deviation between the overall echo intensity and the mean intensity of the subecho is sought when a radar is scanning the homogeneous ground. In the SAR image, it is presented by sharp changes of gray, where some of the resolution units are dark and some are bright, indicating a granular fluctuation. Speckle stems from the associated stacking of radar waves. Generally, speckle noise is asserted to be completely developed. Usually this noise is deemed multiplicative, and the corresponding model is defined as:

$$I(x,y) = R(x,y) \cdot F(x,y), \tag{10}$$

where $I(x,y)$ denotes the SAR intensity image and $R(x,y)$ indicates a noise-free SAR image. $F(x,y)$ refers to the speckle noise with expectation $E = 1$ and variance $Var = \sigma^2$. $R(x,y)$ and $F(x,y)$ are also assumed as mutual independence. To denoise the SAR image easily, logarithmic transform is applied to Eq. (10). Then the additive noise model is attained as follows:

$$\ln(F(x,y)) = \ln(R(x,y)) + \ln(N(x,y)). \tag{11}$$

It is found that the present noise $\ln(N(x,y))$ is approaching Gaussian distribution [20]. The objective for speckle reduction is equal to finding the optimal estimation of $\ln(R(x,y))$ so that the denoising algorithm proposed in this paper can be applied to the model of Eq. (11). In this paper, the steps of the SAR image denoising algorithm are as follows:

1) Use logarithmic transform for the noisy SAR image to obtain the logarithmic image;
2) Apply the NSST to the image;
3) Apply patch ordering to NSST coefficients, and then use the least square method to denoise the coefficients;
4) Reset the denoised patch, i.e. perform patch reordering;
5) Apply inverse NSST to the reordering coefficient;
6) Apply exponential transform to the obtained image and then acquire the ultimate denoised SAR image.

Figure 2 provides the SAR image denoising flow chart of this paper. However, bias would be introduced by homomorphic speckle filtering with a log transformation. This problem arises from the fact that the logarithmic transform is nonlinear, thus leading to uneven filtering. This mean bias is corrected before the final exponential transform step through adding a parameter like in [20], which depends on the mean value of the estimated log-transformed speckle noise.

In our paper, the scale of the NSST decomposition is 2, the first scale contains 4 directions subbands, and the second scale has 8 directions subbands. According to the time and computational complexity of our algorithm, we can get about $13N^2$ shearlet coefficients by applying shearlet analysis to the image with the size of $N \times N$ whose time complexity is $O(N \log N)$. We choose the distance measure ω to be the squared

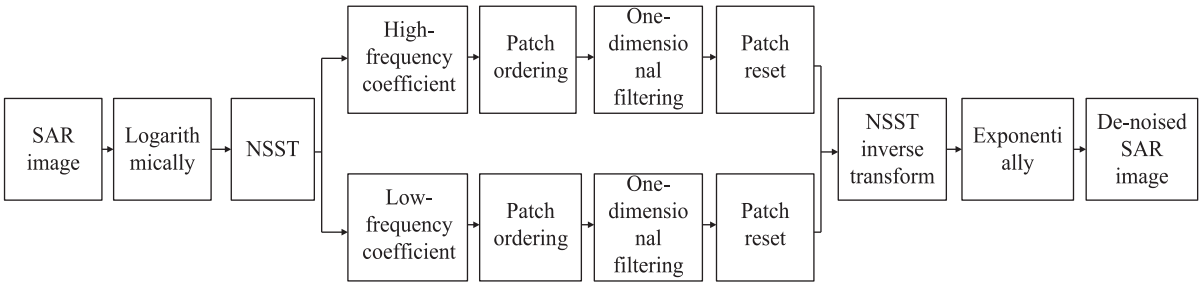

Figure 2. Flow chart of SAR image denoising based on patch ordering in NSST domain.

Euclidean distance, and the computation complexity is K. It is known from Eq. (5) that the sum of path ω of points x_j^p and its neighboring points is $\frac{N^2}{n}K$. Let M denote the computational complexity of minimizing X_{TV}^P and refer to [19]. As known from Eq. (8), the computational complexity of filter coefficients $\hat{h}_j$ is $L \times L$. Then we can obtain the computational complexity of the iterative solution as $\frac{N^2}{n}KML^2$. We can further improve our results by applying a second iteration of our proposed scheme, in which all the processing stages remain the same but the permutation matrices are built using patches extracted from the first iteration's clean result. Thus, the overall computational complexity is about $\mathrm{O}\left(\frac{N^2}{n}KML^2\right)$.

4. Experimental results and analysis

We denoise the original SAR image of TerraSar-X shooting with various approaches and analyze the results to test the reliability and feasibility of the proposed method. The compared SAR image denoising methods are the Lee filter [3], Frost filter [4], Bayesian denoising in wavelet domain (BWS) [6], sparse representation-based Bayesian denoising in shearlet domain (BSSR) [21], SAR image denoising in NSST domain (NSST) [22], generalized nonlocal means-based SAR image denoising in NSST domain (GNL-NSST) [23], and GNL-means-based SAR image denoising with optimized pixel-wise weighting in NSST domain (GNL-OPW) [24]. Figure 3 shows the test images adopted in this paper.

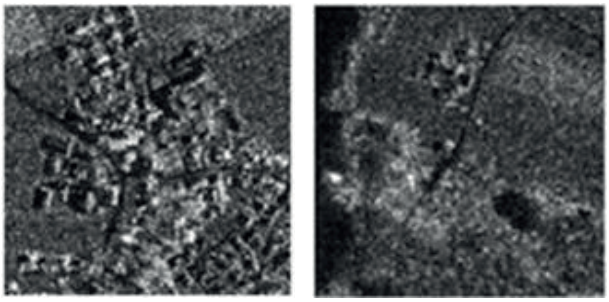

(a) (b)

Figure 3. The actual SAR images: (a) fields, (b) woods.

As indicated, Figure 3a is a SAR image of fields and Figure 3b is a SAR image of woods. Figures 4a–4h show the denoised images of Figure 3a after denoising by the above algorithms. Figures 5a–5h show the denoised images of Figure 3b after denoising by the above algorithms. As acquired from Figures 4 and 5, the Lee filter (see Figures 4a and 5a) and Frost filter (see Figures 4b and 5b) are less effective. In Figures 4c and 5c, some

edge textures are eliminated through adopting BWS. In Figures 4d and 5d, some artificial texture is produced by adopting BSSR. The method of NSST creates edge blur, as seen in Figures 4e and 5e. It is also seen that GNL-NSST removes some textures of the edge in Figures 4f and 5f, and GNL-OPW produces some artificial texture in Figures 4g and 5g. In Figures 4h and 5h, the proposed algorithm can better maintain the image edge and image texture information, simultaneously inhibiting the artificial texture to be further generated. The visual effect is also evidently optimized. This proves that the proposed algorithm outperforms other algorithms.

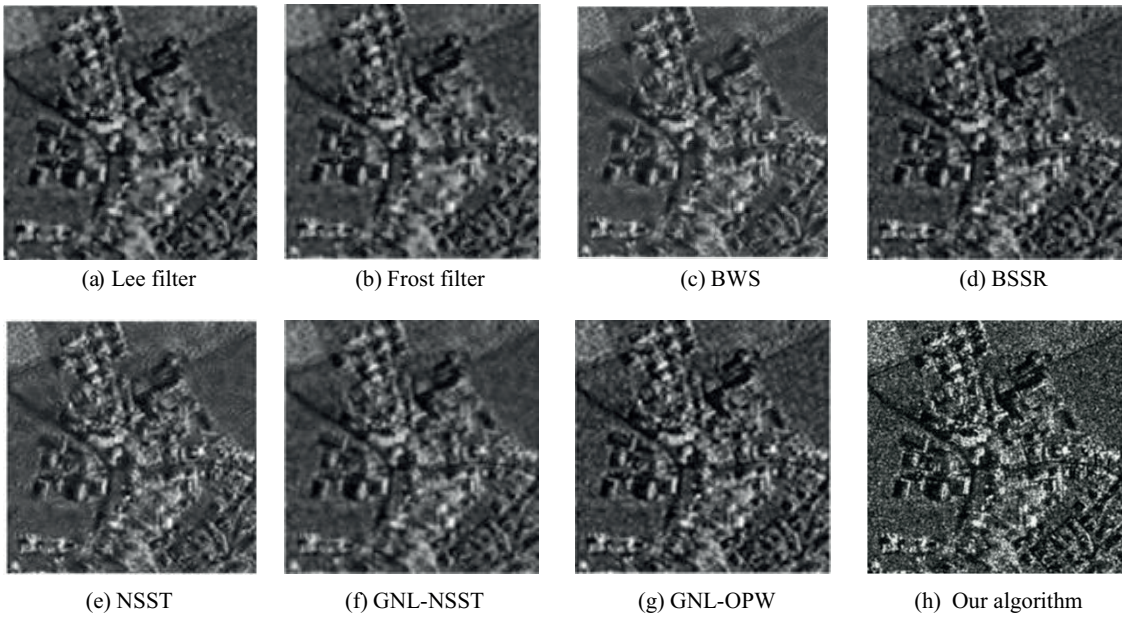

Figure 4. The denoised results of the fields.

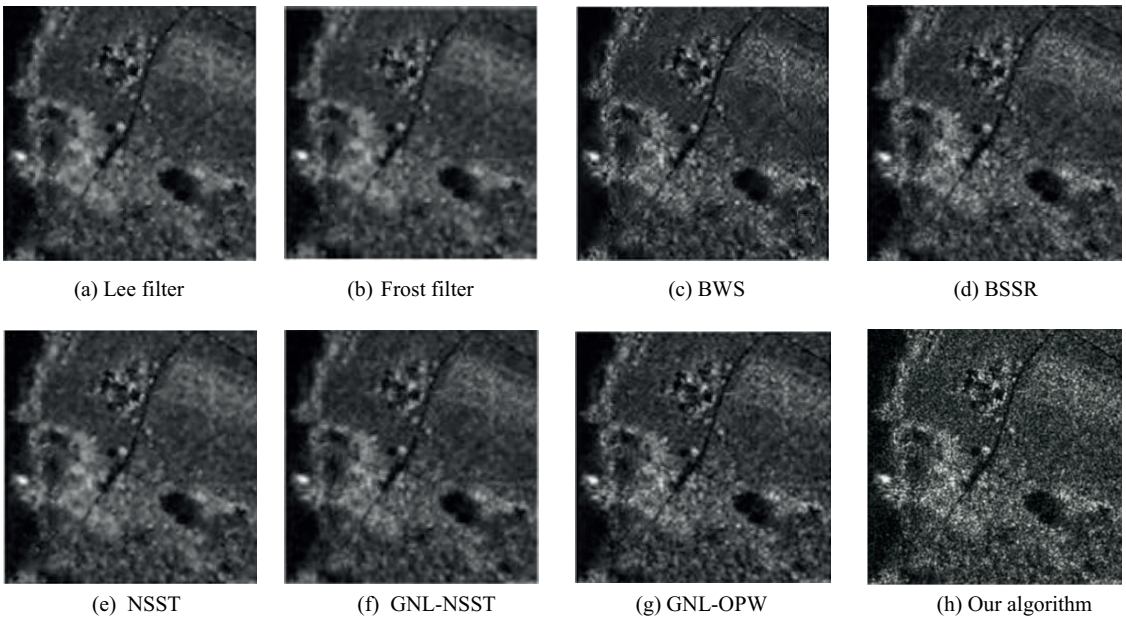

Figure 5. The denoised results of the woods.

Objective evaluation criteria are adopted to assist the subjective evaluation criteria in evaluating the performance of all denoised methods. The common parameters of denoising performance are peak signal to noise ratio (PSNR), edge preservation index (EPI), equivalent number of looks (ENL), and unassisted measure of quality following the first- and second-order descriptors of ratio of denoised image to natural image (UM) [25]. UM is a new evaluation criterion to objectively evaluate despeckling filters. The evaluation relies on measuring deviations from the ideal statistical properties of the ratio image and their residual structural contents. It shows expressiveness and adequacy, and it has been verified that it is consistent with widely used image-quality indices as well as the visual inspection of both filtered and ratio images.

The mathematical expressions of PSNR, EPI, and ENL are as follows:

$$PSNR = \frac{255^2 M \times N}{\sum_{i=1}^{M}\sum_{j=1}^{N} |I(i,j) - \hat{I}(i,j)|^2}, \tag{12}$$

where I denotes the noisy image and $\hat{I}$ denotes the denoised image. (i,j) is the position of the pixel. $M \times N$ indicates the size of the selected image.

$$EPI = \frac{\sum_{i}^{M}\sum_{j}^{N} |\hat{I}(i,j) - 8 * E(\hat{I}_{(i,j)\in\Omega})|}{\sum_{i}^{M}\sum_{j}^{N} |I(i,j) - 8 * E(I_{(i,j)\in\Omega})|}, \tag{13}$$

where Ω represents the window centered at (i,j). $E(\hat{I}_{(i,j)\in\Omega})$ indicates the mean of the pixels in Ω.

$$ENL = \frac{(E(I))^2}{var(I)}, \tag{14}$$

where $var(I)$ denotes the variance and $E(I)$ denotes the mean of the image.

Furthermore, a larger PSNR shows that the denoising ability is strong. The greater the EPI, the more detailed information is retained by the algorithm. A larger ENL takes on better visual effects. As indicated from the smaller UM, the denoising algorithm is advantageous in performance. The performance parameters are shown in the Table.

Table. Performance parameters of the denoising methods in Figures 4 and 5.

Denoising methods	Parameters in Figure 4				Parameters in Figure 5			
	UM	PSNR	ENL	EPI	UM	PSNR	ENL	EPI
Lee filter	7.70	28.28	7.35	0.67	7.73	29.05	6.35	0.80
Frost filter	7.56	27.28	7.44	0.68	7.75	28.05	27.15	0.72
BWS	7.23	30.75	12.75	0.85	7.42	32.78	10.55	0.89
BSSR	6.34	34.33	19.90	0.94	6.56	35.85	24.19	0.97
NSST	6.99	31.55	15.56	0.88	7.32	33.11	22.45	0.90
GNL-NSST	5.78	35.01	20.65	0.95	5.67	36.67	25.55	0.98
GNL-OPW	5.70	35.13	21.05	0.96	5.63	36.78	26.57	0.98
Our algorithm	4.56	35.99	21.88	0.97	4.75	37.18	27.78	0.99

As indicated in the Table, the proposed algorithm takes on the optimal UM, PSNR, and ENL, and the EPI is approaching 1. Therefore, our SAR image denoising algorithm outperforms the others.

Through comprehensively analyzing the foregoing information, this paper shows that the proposed algorithm to denoise the SAR image not only has a strong ability to denoise and provide preferable visual effects, but it can also better preserve the texture information of a SAR image.

5. Conclusion

To smooth the speckle in a SAR image, a novel algorithm is proposed to denoise the SAR image based on patch ordering in the NSST domain. We introduce the patch ordering that has carefully designed permutation matrices and simple and intuitive 1D operations. For a given corrupted image, we no longer apply patch ordering directly to the image. Instead, we apply the NSST to the image to process the NSST coefficients. As the experimental results demonstrate, the proposed algorithm outperforms the traditional algorithms in denoising. This algorithm not merely suppresses and eliminates the speckle noise effectively, but also preserves the texture information of the image more efficiently. In future research, we will study how to reduce the computational complexity of the algorithm.

6. Acknowledgment

This work was supported in part by the Natural Science Foundation of China under grants 61401308 and 61572063, the Natural Science Foundation of Hebei Province under grants F2016201142 and F2016201187, the Science Research Project of Hebei Province under grant QN2016085, the Natural Science Foundation of Hebei University under grant 2014-303, and the Post-Graduate's Innovation Fund Project of Hebei University under grants X201710 and hbu2018ss01.

References

[1] Wang Y, Ainsworth TL, Lee JS. Application of mixture regression for improved polarimetric SAR speckle filtering. IEEE T Geosci Remote 2016; 55: 453-467.

[2] Lobry S, Denis L, Tupin F. Multitemporal SAR image decomposition into strong scatterers, background, and speckle. IEEE J-Stars 2016; 9: 3419-3429.

[3] Lee JS, Jurkevich L, Dewaele P, Wambacq P, Oosterlinck A. Speckle filtering of synthetic aperture radar images: a review. Remote Sensing Reviews 1994; 8: 255-267.

[4] Frost VS, Stiles JA, Shanmugan KS, Holtzman JC. A model for radar image and its application to adaptive digital filtering of multiplicative noise. IEEE T Pattern Anal 2009; 4: 157-166.

[5] Martino GD, Simone AD, Iodice A, Riccio D. Scattering-based nonlocal means SAR despeckling. IEEE T Geosci Remote 2016; 54: 3574-3588.

[6] Dai M, Peng C, Chan AK, Loguinov D. Bayesian wavelet shrinkage with edge detection for SAR image despeckling. IEEE T Geosci Remote 2004; 42: 1642-1648.

[7] Fang J, Wang D, Xiao Y, Saikrishna DA. De-noising of SAR images based on Wavelet-Contourlet domain and PCA. In: IEEE 2015 International Conference on Signal Processing; 25–26 April 2015; Beijing, China. New York, NY, USA: IEEE. pp. 942-945.

[8] Liu SQ, Liu M, Li P, Zhao J, Zhu ZH, Wang XH. SAR image denoising via sparse representation in Shearlet domain based on continuous cycle spinning. IEEE T Geosci Remote 2017; 55: 2985-2992.

[9] Karami A, Heylen R, Scheunders P. Band-specific shearlet-based hyperspectral image noise reduction. IEEE T Geosci Remote 2015; 53: 5054-5066.

[10] Lim WQ. The discrete shearlets transform: a new directional transform and compactly supported shearlets frames. IEEE T Image Process 2010; 19: 1166-1180.

[11] Sharifymoghaddam M, Beheshti S, Elahi P, Hashemi M. Similarity validation based nonlocal means image denoising. IEEE Signal Proc Let 2015; 22: 2185-2188.

[12] Chatterjee P, Milanfar P. Clustering-based de-noising with locally learned dictionaries. IEEE T Image Process 2009; 18: 1438-1451.

[13] Yu G, Sapiro G, Mallat S. Solving inverse problems with piecewise linear estimators: from Gaussian mixture models to structured sparsity. IEEE T Image Process 2012; 21: 2481-2499.

[14] Zoran D, Weiss Y. From learning models of natural image patches to whole image restoration. In: IEEE 2011 International Conference on Computer Vision; 6–13 November 2011; Barcelona, Spain. New York, NY, USA: IEEE. pp. 479-486.

[15] Elad M, Aharon M. Image de-noising via sparse and redundant representations over learned dictionaries. IEEE T Image Process 2006; 15: 3736-3745.

[16] Rasti B, Ulfarsson MO, Ghamisi P. Automatic hyperspectral image restoration using sparse and low-rank modeling. IEEE Geosci Remote S 2017; 14: 2335-2339.

[17] Dabov K, Foi A, Katkovnik V, Egiazarian K. Image de-noising by sparse 3-D transform-domain collaborative filtering. IEEE T Image Process 2007; 16: 2080-2095.

[18] Ram I, Cohen I, Elad M. Patch-ordering-based wavelet frame and its use in inverse problems. IEEE T Image Process 2014; 23: 2779-2792.

[19] Ram I, Elad M, Cohen I. Redundant wavelets on graphs and high dimensional data clouds. IEEE Signal Proc Let 2012; 19: 291-294.

[20] Xue B, Huang Y, Yang J, Shi L, Zhan Y, Cao X. Fast nonlocal remote sensing image denoising using cosine integral images. IEEE Geosci Remote S 2013; 10: 1309-1313.

[21] Liu SQ, Hu SH, Xiao Y, An YL. Bayesian Shearlet shrinkage for SAR image de-noising via sparse representation. Multidim Syst Sign P 2014; 25: 683-701.

[22] Fabbrini L, Greco M, Messina M, Pinelli G. Improved anisotropic diffusion filtering for SAR image despeckling. Electron Lett 2013; 49: 672-674.

[23] Liu SQ, Geng P, Shi M, Fang J, Hu S. SAR image de-noising based on generalized non-local means in non-subsample Shearlet domain. In: CSPS 2015 International Conference on Communications, Signal Processing, and Systems; 23–24 October 2015; Sichuan, China. Berlin, Germany: CSPS. pp. 221-229.

[24] Liu SQ, Zhang Y, Hu Q, Liu M, Zhao J. SAR image de-noising based on GNL-means with optimized pixel-wise weighting in non-subsample shearlet domain. Stud Comp Intell 2017; 10: 16-22.

[25] Gomez L, Ospina R, Frery AC. Unassisted quantitative evaluation of despeckling filters. Remote Sens-Basel 2017; 9: 389-392.